Effect of Pt substitution on the electronic structure of $AuTe_2$

D. Ootsuki,[1] K. Takubo,[2,3,4] K. Kudo,[5] H. Ishii,[5] M. Nohara,[5] N. L. Saini,[6] R. Sutarto,[7] F. He,[7] T. Z. Regier,[7] M. Zonno,[2] M. Schneider,[2] G. Levy,[2,3] G. A. Sawatzky,[2,3] A. Damascelli,[2,3] and T. Mizokawa[1,6]

[1]*Department of Physics & Department of Complexity Science and Engineering, University of Tokyo, 5-1-5 Kashiwanoha, Chiba 277-8561, Japan*

[2]*Department of Physics & Astronomy, University of British Columbia, Vancouver, British Columbia, Canada V6T 1Z1*

[3]*Quantum Matter Institute, University of British Columbia, Vancouver, British Columbia, Canada V6T 1Z4*

[4]*Max Planck Institute for Solid State Research, Heisenbergstrasse 1, D-70569 Stuttgart, Germany*

[5]*Department of Physics, Okayama University, 3-1-1 Tsushima-naka, Kita-ku, Okayama 700-8530, Japan*

[6]*Department of Physics, University of Rome "La Sapienza," 00185 Rome, Italy*

[7]*Canadian Light Source, Saskatoon, Saskatchewan, Canada S7N 2V3*

(Received 1 July 2014; revised manuscript received 9 October 2014; published 27 October 2014)

We report a photoemission and x-ray absorption study on a $Au_{1-x}Pt_xTe_2$ ($x = 0$ and 0.35) triangular lattice in which superconductivity is induced by Pt substitution for Au. Au $4f$ and Te $3d$ core-level spectra of $AuTe_2$ suggest a valence state of $Au^{2+}(Te_2)^{2-}$, which is consistent with its distorted crystal structure with Te-Te dimers and compressed $AuTe_6$ octahedra. On the other hand, valence-band photoemission spectra and preedge peaks of the Te $3d$ absorption edge indicate that Au $5d$ bands are almost fully occupied and that Te $5p$ holes govern the transport properties and the lattice distortion. The two apparently conflicting pictures can be reconciled by strong Au $5d$/Au $6s$–Te $5p$ hybridization. The absence of a core-level energy shift with Pt substitution is inconsistent with the simple rigid band picture for hole doping. The Au $4f$ core-level spectrum gets slightly narrow with Pt substitution, indicating that the small Au $5d$ charge modulation in distorted $AuTe_2$ is partially suppressed.

DOI: 10.1103/PhysRevB.90.144515 PACS number(s): 74.25.Jb, 74.70.Xa, 74.70.Dd, 78.70.Dm

I. INTRODUCTION

Layered transition-metal dichalcogenides with a triangular motif have been attracting renewed interest due to the discovery of superconductivity in chemically substituted $IrTe_2$ [1–4] and $AuTe_2$ [5] with a maximum T_c of 3.1 and 4.0 K, respectively. In particular, the electronic structure of $IrTe_2$ and its derivatives has been studied intensively using various spectroscopic methods under anticipation that the strong spin-orbit interaction in the Ir $5d$ and Te $5p$ orbitals may provide a novel spin-momentum entangled quantum state [6–9]. Also details of the structural transition in $IrTe_2$ [10,11] have been revealed by recent studies using advanced x-ray diffraction and scattering techniques [12–16]. On the other hand, so far, electronic structure studies on $AuTe_2$ and its derivatives have been limited, although the Au $5d$ and/or Te $5p$ electrons with strong spin-orbit interaction can provide an interesting electronic state.

$AuTe_2$ is known as a natural mineral Calaverite with a monoclinically distorted CdI_2-type layered structure (space group $C2/m$) [17]. Each Au-Te layer contains edge-shared $AuTe_6$ octahedra that are strongly distorted with two short (2.67 Å) and four long (2.98 Å) Au-Te bonds due to Te-Te dimer formation in the average structure [17,18]. A detailed analysis of the crystal structure has revealed incommensurate structural modulation, which may indicate charge ordering of Au $5d$ and/or Te $5p$ valence electrons [19]. Although Au^+/Au^{3+} charge disproportionation has been suggested to explain the structural distortion [19], the expected Au valence modulation has not been detected by x-ray photoemission spectroscopy [20]. In addition, *ab initio* calculations have indicated that the Au $5d$ subshell is almost fully occupied by electrons, and the Te-Te dimer formation due to the partially occupied Te $5p$ subshell should be responsible for the structural distortion [21]. Very recently, Kudo *et al.* have found that Pt substitution for Au suppresses the lattice distortion of $AuTe_2$, and that $Au_{1-x}Pt_xTe_2$ with an undistorted CdI_2-type ($P\bar{3}m1$) structure exhibits superconductivity with a maximum T_c of 4.0 K [5]. The electronic phase diagram for $Au_{1-x}Pt_xTe_2$ is similar to $Ir_{1-x}Pt_xTe_2$, indicating an intimate relationship between the lattice distortion in $AuTe_2$ and the superconductivity in $Au_{1-x}Pt_xTe_2$. In the present work, we have studied the fundamental electronic structure of $Au_{1-x}Pt_xTe_2$ ($x = 0$ and 0.35) by means of ultraviolet photoemission spectroscopy (UPS), x-ray photoemission spectroscopy (XPS), and x-ray absorption spectroscopy (XAS). The valence-band UPS and XPS results show that the Au $5d$ and Te $5p$ orbitals are strongly hybridized near the Fermi level. The core-level XPS results indicate small charge distribution of the Au $5d$ electrons, which is suppressed by the Pt substitution. The active role of the Te $5p$ holes is indicated by the Te $3d$ XAS measurement.

II. EXPERIMENTS

The polycrystalline samples of $Au_{1-x}Pt_xTe_2$ ($x = 0.35$, $T_c = 4.0$ K) and single crystals of $AuTe_2$ were prepared as reported in the literature [5]. Single crystals of $AuTe_2$ were cleaved for UPS and XAS at 300 K. UPS measurements were performed at UBC using a SPECS Phoibos 150 analyzer with the He I line (21.2 eV) from a monochromatized UVS300 lamp. The total energy resolution was set to 25 meV. The base pressure was in the 10^{-11} mbar range. XAS measurements were performed at beamlines 11ID-1 and 10ID-2 [22], Canadian Light Source. The total-energy resolution was 100 meV. The base pressure of the XAS chamber was in the 10^{-9} mbar range. The spectra were measured in the total-electron-yield (TEY) mode. XPS measurements were carried out using a JEOL JPS9200 analyzer. Mg $K\alpha$ (1253.6 eV) was used as an x-ray

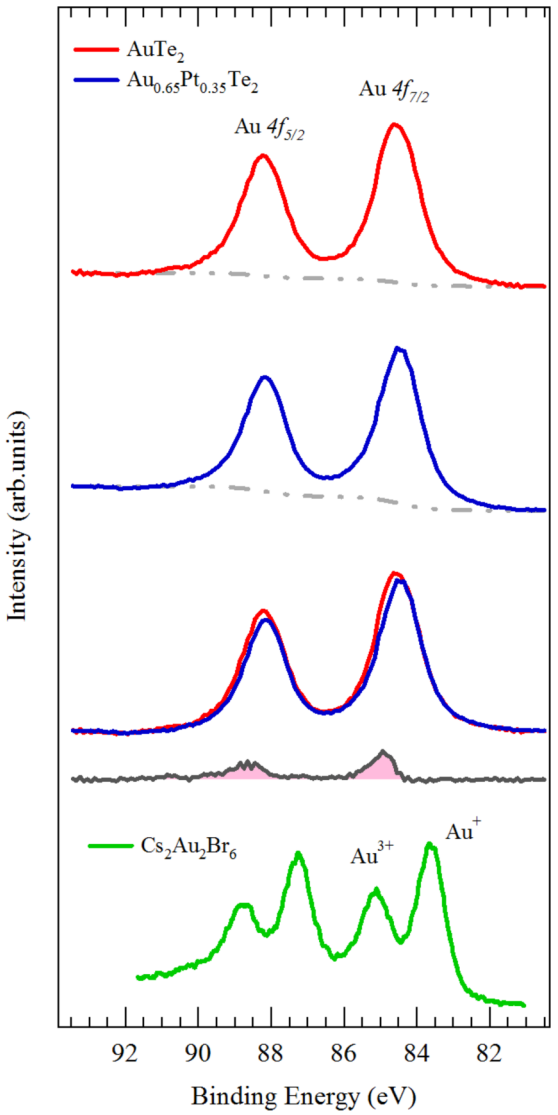

FIG. 1. (Color online) Au $4f$ core-level XPS spectra of $AuTe_2$ and $Au_{0.65}Pt_{0.35}Te_2$ compared with $Cs_2Au_2Br_6$ [23]. The dash-dot curves indicate backgrounds due to secondary electrons. The background-subtracted spectra of $Au_{0.65}Pt_{0.35}Te_2$ are overlaid with that of $AuTe_2$, and the difference between the background-subtracted spectra is indicated by the solid curve with shaded peak area.

source. The total energy resolution was set to ~1.0 eV, and the binding energy was calibrated using the Au $4f$ core level of the gold reference sample at 84.0 eV. The polycrystalline sample of $Au_{1-x}Pt_xTe_2$ ($x = 0.35$) and single crystal of $AuTe_2$ were fractured *in situ* at 300 K for the XPS measurements.

III. RESULTS AND DISCUSSION

Figure 1 shows the Au $4f$ core-level spectra of $Au_{1-x}Pt_xTe_2$ ($x = 0$ and 0.35) taken at 300 K, which are compared with $Cs_2Au_2Br_6$ with Au^+ and Au^{3+} sites. The broad Au $4f_{7/2}$ peak of $AuTe_2$ would be consistent with the Au valence modulation due to the lattice distortion. However, the Au $4f_{7/2}$ peak width of $Au_{0.65}Pt_{0.35}Te_2$ without the distortion is also comparable to that of $AuTe_2$. While the formal valence of Au is +4 in $Au_{1-x}Pt_xTe_2$, the Au $4f_{7/2}$ peaks are slightly higher in binding energy than that of pure Au (84.0 eV) and located between the Au^+ and Au^{3+} peaks of $Cs_2Au_2Br_6$, suggesting that the actual average Au valence in $Au_{1-x}Pt_xTe_2$ is close to 2+. Although the Au^{2+} ion is expected to take the $5d^9$ configuration, the band-structure calculations on the average structure indicate that the Au $5d$ bands are almost fully occupied [21,24].

The Te $3d$ core-level spectra of $Au_{1-x}Pt_xTe_2$ ($x = 0$ and 0.35) are displayed in Fig. 2. The binding energy of the Te $3d_{5/2}$ core level is close to that of pure Te (573.0 eV) [25], suggesting that the Te $5p$ orbitals are not fully occupied and contribute to the electronic states at the Fermi level. The shoulder structures located at ~576 and ~587 eV for Te $3d_{5/2}$ and Te $3d_{3/2}$ are derived from Te oxide contaminations, which were also observed in the $IrTe_2$ single crystals and the $Ir_{1-x}Pt_xTe_2$ polycrystalline samples [6]. The shoulder structures in the $AuTe_2$ single crystal and the polycrystalline $Au_{1-x}Pt_xTe_2$ are much smaller than that in the polycrystalline $Ir_{1-x}Pt_xTe_2$ and are as small as that in the high-quality $IrTe_2$ single crystal, indicating that the surface quality of $AuTe_2$ and $Au_{1-x}Pt_xTe_2$ is reasonably good.

To clarify the effect of Pt substitution, we have subtracted the core-level spectrum of $Au_{0.65}Pt_{0.35}Te_2$ from that of $AuTe_2$ as displayed in Figs. 1 and 2 . The Au $4f$ and Te $3d$ core-level peaks do not show an appreciable energy shift with the Pt substitution. The difference spectrum shows that the Au $4f$ core-level spectrum of $AuTe_2$ gets slightly narrow with the Pt substitution, while it does not affect the Te $3d$ core level appreciably. This indicates small Au $5d$ charge modulation in distorted $AuTe_2$ and partial suppression of the charge modulation by the Pt substitution. Here, one cannot fully exclude the possibility that the Au valence at the surface is different from the bulk and that the surface component is enhanced in $AuTe_2$. However, the surface condition of the $AuTe_2$ single crystal is expected to be better than $Au_{0.65}Pt_{0.35}Te_2$, and the surface component in $AuTe_2$ should be smaller than the polycrystalline case if it exists. On the other hand, the Au $4f$ peak is broader in the $AuTe_2$ single crystal than the polycrystalline case. Therefore, it is natural to assign the extra broadening in $AuTe_2$ to the extra charge modulation instead of the surface effect.

In Fig. 3, valence-band XPS and UPS spectra of $Au_{1-x}Pt_xTe_2$ ($x = 0$ and 0.35) taken at 300 K are displayed. The valence-band UPS and XPS spectra of $Au_{1-x}Pt_xTe_2$ show several structures. The broad structures ranging from 0 to 4 eV below the Fermi level can be assigned to the Te $5p$ orbitals (mixed with the Au $5d/6s$ orbitals) on the basis of the band-structure calculations on $AuTe_2$ [21,24]. The structures from 4.0 to 6.5 eV can be assigned to the Au $5d$ bands since they gain spectral weight in going from UPS to XPS, as expected from the photon energy dependence of the photoionization cross section of Au $5d$ relative to Te $5p$. Indeed, the valence-band spectra are consistent with the calculated density of states [24] in which the Au $5d$ bands are located in the region from 4.0 to 6.0 eV below the Fermi level. The valence-band spectra of $Au_{0.65}Pt_{0.35}Te_2$ are shifted toward lower binding energy, indicating that the Pt substitution for Au may correspond to hole doping to the Te $5p$ bands mixed with the Au $5d/6s$ orbitals. Another possibility is that mixing of the

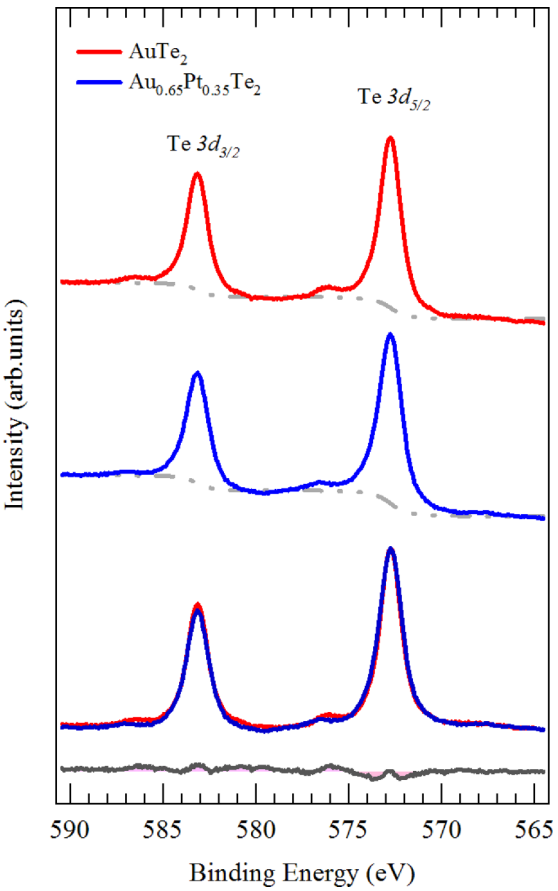

FIG. 2. (Color online) Te $3d$ core-level XPS spectra of $AuTe_2$ and $Au_{0.65}Pt_{0.35}Te_2$. The dash-dot curves indicate background due to secondary electrons. The background subtracted spectra of $Au_{0.65}Pt_{0.35}Te_2$ are overlaid with that of $AuTe_2$, and the difference spectrum between the background-subtracted spectra is indicated by the solid curve with a shaded peak area.

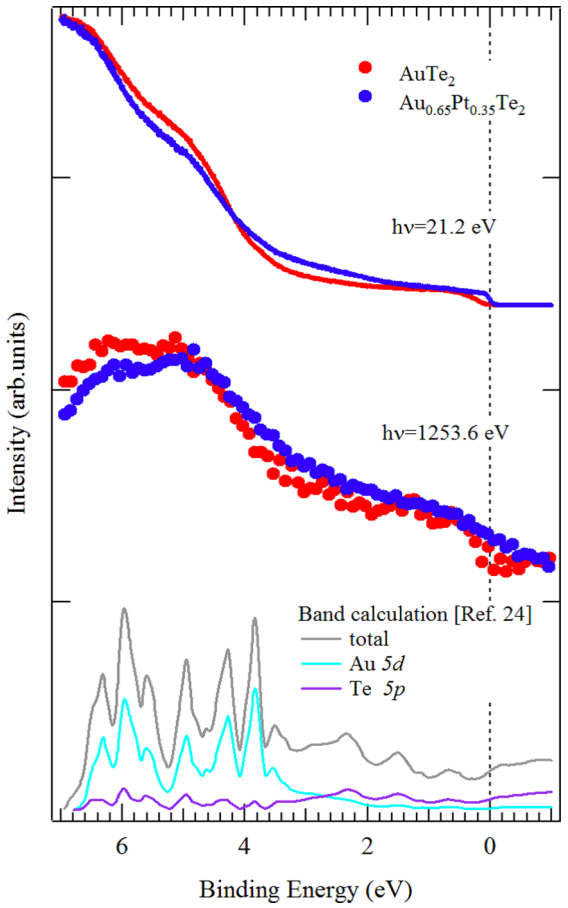

FIG. 3. (Color online) Valence-band UPS and XPS spectra of $AuTe_2$ and $Au_{0.65}Pt_{0.35}Te_2$ compared with the total and partial density of states of $AuTe_2$ [24].

Au $5d$ bands with the Pt $5d$ bands leads to the energy shift of the Au/Pt $5d$ bands since the Pt $5d$ bands are expected to have lower binding energy than the Au $5d$ bands. The absence of the core-level energy shift is inconsistent with the former scenario (hole doping in a rigid band manner) and supports the latter scenario, namely that the Pt substitution changes the shape of the valence band constructed from the Au/Pt $5d/6s$ and Te $5p$ orbitals, and it cannot be viewed as a simple hole doping to $AuTe_2$ in a rigid band manner.

The average Au valence close to $+2$ and the unoccupied Te $5p$ orbitals indicate that the charge-transfer energy from the Te $5p$ orbitals to the Au $5d$ orbitals is negative to stabilize the valence state of $Au^{2+}(Te_2)^{2-}$. Namely, the local electronic configuration of the $AuTe_6$ octahedron is close to $d^9\underline{L}^2$ ($\underline{L}$ represents a ligand hole in the Te $5p$ orbitals) instead of d^7. Therefore, each Te site accommodates approximately one hole, and the Te $5p$ holes govern the transport properties and the lattice distortions in $AuTe_2$. This picture is consistent with the Te-Te dimers in $AuTe_2$ since the antibonding molecular orbital of the Te-Te dimer can be occupied by the two Te $5p$ holes from the two Te sites. On the other hand, the band-structure calculations on $AuTe_2$ with the average structure [21,24] as well as the valence-band spectra indicate that the Au $5d$ bands are almost fully occupied. To resolve this apparent paradox, strong hybridization between the Au $5d/6s$ and Te $5p$ orbitals should be taken into account. Starting from the $Au^{2+}(Te_2)^{2-}$ valence state, the hybridization between the Au $5d/6s$ orbitals and the Te-Te bonding and antibonding molecular orbitals can induce additional charge transfer. Since the Au $5d$ level in $AuTe_2$ is much lower than the Ir $5d$ level in $IrTe_2$, charge donation from the Te-Te bonding orbital to the Au $5d$ orbitals can be dominant in $AuTe_2$, whereas back donation from the Ir $5d$ orbitals to the Te-Te antibonding orbital would be substantial in $IrTe_2$. In addition, the Au $6s$ component can be mixed into the Au $5d$ bands through the strong Au $5d$-Te $5p$ and Te $5p$-Au $6s$ hybridizations. Therefore, although the "Au $5d$ bands" constructed from the atomic Au $5d$, Au $6s$, and Te $5p$ orbitals are fully occupied, as predicted by the band-structure calculations and observed by the valence-band photoemission experiments, the actual number of atomic Au $5d$ electrons in $AuTe_2$ can remain close to nine, which is consistent with the $Au^{2+}(Te_2)^{2-}$ valence state. The d^9 configuration of Au^{2+} is consistent with the Jahn-Teller-like distortion of the $AuTe_6$ octahedra with two short and four long Au-Te bonds.

Figure 4 shows the Te $3d$ XAS spectrum of $Au_{1-x}Pt_xTe_2$ ($x = 0$ and 0.35). The preedge and main edge structures are clearly observed. The main-edge structure corresponds to the

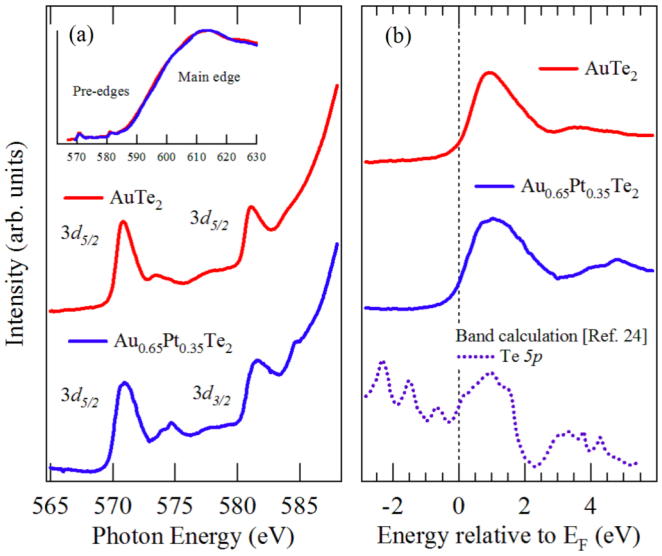

FIG. 4. (Color online) (a) Te $3d$ XAS spectrum of $AuTe_2$ and $Au_{0.65}Pt_{0.35}Te_2$. The inset shows the wide-range XAS spectrum including the main edge. (b) The Te $3d_{5/2}$ XAS spectrum is compared with the calculated density of states [24]. Here, it is assumed that the Fermi level is roughly located around the absorption edge.

transition from the Te $3d$ core level to the unoccupied Te $4f$/Au $6s$,$6p$ states. On the other hand, the preedge structure can be assigned to the transition from the Te $3d$ core level to the Te $5p$ orbitals, indicating that the Te $5p$ bands cross the Fermi level and that the Te $5p$ holes play essential roles in the transport properties. This Te $5p$–hole picture is consistent with the XPS and XAS results. In $AuTe_2$, the Te $5p$ orbitals are partially unoccupied, and the bond formation by the Te $5p$ holes creates the Te-Te dimers. The Te-Te dimer formation leads to the long and short Te-Te bonds [17,18], which can induce charge modulation of Au through the strong hybridization between the Au $5d$ and Te $5p$ orbitals. On the other hand, since all the Te sites belong to one of the Te-Te dimers, each Te site accommodates almost the same amount of Te $5p$ hole. When Pt is substituted for Au in $Au^{2+}(Te_2)^{2-}$, Pt ions tend to be 3+ or 4+ and supply electrons to Te-Te antibonding orbitals. Consequently, the local Te-Te dimers are partly broken around the Pt sites, and the superstructure due to the short Te-Te bond (intradimer) and long Te-Te bond (interdimer) is strongly disturbed. In this scenario, disordered local Te-Te dimers can remain in $Au_{1-x}Pt_xTe_2$. The remaining Au charge fluctuation and the disordered Te-Te dimers may provide anomalous lattice behaviors to $Au_{1-x}Pt_xTe_2$ and may contribute to the emergence of superconductivity [5].

IV. CONCLUSION

We have performed photoemission and x-ray absorption measurements on $Au_{1-x}Pt_xTe_2$ ($x = 0$ and 0.35) in which the Pt substitution for Au suppresses the lattice distortion in $AuTe_2$ and induces superconductivity. The broad Au $4f$ core-level peak is consistent with the Au valence modulation in distorted $AuTe_2$. The Au $4f$ core-level peak gets slightly narrow with the Pt substitution, indicating that small Au $5d$ charge modulation in distorted $AuTe_2$ is at least partially suppressed by the Pt substitution. The Au $4f$ and Te $3d$ core-level binding energies suggest that the average valence state is close to $Au^{2+}(Te_2)^{2-}$, consistent with the Jahn-Teller-like distortion of the $AuTe_6$ octahedra. On the other hand, the valence-band spectra and the band-structure calculations show that the Au $5d$ bands are almost fully occupied. The two apparently conflicting results can be reconciled by taking account of the strong Au $5d$/Au $6s$–Te $5p$ hybridization. The absence of a core-level energy shift with the Pt substitution shows that the simple rigid band picture is not applicable to $Au_{1-x}Pt_xTe_2$. Although the periodic arrangement of the Te-Te dimers is disturbed by the Pt substitution, the Te-Te dimers and Au valence modulation may partly remain in superconducting $Au_{1-x}Pt_xTe_2$. The relationship between the possible Au charge fluctuation and the superconductivity should be studied experimentally and theoretically in the future. Another interesting question is whether the Te-Te dimers still remain in $Au_{1-x}Pt_xTe_2$. If the Pt substitution causes disordering of the dimers instead of breaking, $Au_{1-x}Pt_xTe_2$ should have highly inhomogeneous electronic states similar to the Fe-based superconductors.

ACKNOWLEDGMENTS

The authors would like to thank Y. Ohta and T. Toriyama for informative discussion. This work was partially supported by Grants-in-Aid from the Japan Society of the Promotion of Science (JSPS) (Grants No. 22540363, No. 25400372, No. 25400356, and No. 26287082) and the Funding Program for World-Leading Innovative R&D on Science and Technology (FIRST Program) from JSPS. D.O. acknowledges support from the JSPS Research Fellowship for Young Scientists. The work at UBC was supported by the Max Planck–UBC Centre for Quantum Materials, the Killam, Alfred P. Sloan, Alexander von Humboldt, and NSERC's Steacie Memorial Fellowships (A.D.), the Canada Research Chairs Program (A.D., G.A.S.), NSERC, CFI, and CIFAR Quantum Materials. The XAS experiments were carried out at beamline 11ID-1 and 10ID-2, Canadian Light Source (Proposals ID: 16-4388 and 18-5295). Part of the research described in this paper was performed at the Canadian Light Source, which is funded by the CFI, NSERC, NRC, CIHR, the Government of Saskatchewan, WD Canada, and the University of Saskatchewan.

[1] S. Pyon, K. Kudo, and M. Nohara, J. Phys. Soc. Jpn. **81**, 053701 (2012).

[2] J. J. Yang, Y. J. Choi, Y. S. Oh, A. Hogan, Y. Horibe, K. Kim, B. I. Min, and S-W. Cheong, Phys. Rev. Lett. **108**, 116402 (2012).

[3] K. Kudo, M. Kobayashi, S. Pyon, and M. Nohara, J. Phys. Soc. Jpn. **82**, 085001 (2013).

[4] M. Kamitani, M. S. Bahramy, R. Arita, S. Seki, T. Arima, Y. Tokura, and S. Ishiwata, Phys. Rev. B **87**, 180501(R) (2013).

[5] K. Kudo, H. Ishii, M. Takasuga, K. Iba, S. Nakano, J. Kim, A. Fujiwara, and M. Nohara, J. Phys. Soc. Jpn. **82**, 063704 (2013).
[6] D. Ootsuki, Y. Wakisaka, S. Pyon, K. Kudo, M. Nohara, M. Arita, H. Anzai, H. Namatame, M. Taniguchi, N. L. Saini, and T. Mizokawa, Phys. Rev. B **86**, 014519 (2012).
[7] A. F. Fang, G. Xu, T. Dong, P. Zheng, and N. L. Wang, Sci. Rep. **3**, 1153 (2013).
[8] D. Ootsuki, S. Pyon, K. Kudo, M. Nohara, M. Arita, H. Anzai, H. Namatame, M. Taniguchi, N. L. Saini, and T. Mizokawa, J. Phys. Soc. Jpn. **82**, 093704 (2013).
[9] Y. S. Oh, J. J. Yang, Y. Horibe, and S.-W. Cheong, Phys. Rev. Lett. **110**, 127209 (2013).
[10] S. Jobic, P. Deniard, R. Brec, J. Rouxel, A. Jouanneaux, and A. N. Fitch, Z. Anorg. Allg. Chem. **598**, 199 (1991).
[11] N. Matsumoto, K. Taniguchi, R. Endoh, H. Takano, and S. Nagata, J. Low Temp. Phys. **117**, 1129 (1999).
[12] A. Kiswandhi, J. S. Brooks, H. B. Cao, J. Q. Yan, D. Mandrus, Z. Jiang, and H. D. Zhou, Phys. Rev. B **87**, 121107(R) (2013).
[13] B. Joseph, M. Bendele, L. Simonelli, L. Maugeri, S. Pyon, K. Kudo, M. Nohara, T. Mizokawa, and N. L. Saini, Phys. Rev. B **88**, 224109 (2013).
[14] T. Toriyama, M. Kobori, Y. Ohta, T. Konishi, S. Pyon, K. Kudo, M. Nohara, K. Sugimoto, T. Kim, and A. Fujiwara, J. Phys. Soc. Jpn. **83**, 033701 (2014).
[15] G. L. Pascut, K. Haule, M. J. Gutmann, S. A. Barnett, A. Bombardi, S. Artyukhin, T. Birol, D. Vanderbilt, J. J. Yang, S.-W. Cheong, and V. Kiryukhin, Phys. Rev. Lett. **112**, 086402 (2014).
[16] K. Takubo, R. Comin, D. Ootsuki, T. Mizokawa, H. Wadati, Y. Takahashi, G. Shibata, A. Fujimori, R. Sutarto, F. He, S. Pyon, K. Kudo, M. Nohara, G. Levy, I. S. Elfimov, G. A. Sawatzky, and A. Damascelli, Phys. Rev. B **90**, 081104(R) (2014).
[17] G. Tunell and L. Pauling, Acta Crystallogr. **5**, 375 (1952).
[18] A. Janner and B. Dam, Acta Crystallogr. Sect. A **45**, 115 (1989).
[19] W. J. Schutte and J. L. de Boer, Acta Crystallogr. Sect. B **44**, 486 (1988).
[20] A. van Triest, W. Folkerts, and C. Haas, J. Phys.: Condens. Matter **2**, 8733 (1990).
[21] B. C. H. Krutzen and J. E. Inglesfield, J. Phys.: Condens. Matter **2**, 4829 (1990).
[22] D. G. Hawthorn, F. He, L. Venema, H. Davis, A. J. Achkar, J. Zhang, R. Sutarto, H. Wadati, A. Radi, T. Wilson, G. Wright, K. M. Shen, J. Geck, H. Zhang, V. Novk, and G. A. Sawatzky, Rev. Sci. Instrum. **82**, 073104 (2011).
[23] J.-Y. Son, T. Mizokawa, J. W. Quilty, K. Takubo, K. Ikeda, and N. Kojima, Phys. Rev. B **72**, 235105 (2005).
[24] S. Kitagawa, H. Kotegawa, H. Tou, H. Ishii, K. Kudo, M. Nohara, and H. Harima, J. Phys. Soc. Jpn. **82**, 113704 (2013).
[25] R. Nyholm and N. Mårtensson, J. Phys. C **13**, L279 (1980).